Suppressed Quenching and Strong-Coupling of Purcell-Enhanced Single-Molecule Emission in Plasmonic Nanocavities

Nuttawut Kongsuwan,[†] Angela Demetriadou,[†] Rohit Chikkaraddy,[‡] Felix Benz,[‡] Vladimir A. Turek,[‡] Ulrich F. Keyser,[‡] Jeremy J. Baumberg,[*,‡] and Ortwin Hess[*,†]

[†]*Blackett Laboratory, Prince Consort Road, Imperial College London, London SW7 2AZ, UK*

[‡]*Cavendish Laboratory, University of Cambridge, Cambridge CB3 0HE, UK*

E-mail: jjb12@cam.ac.uk; o.hess@imperial.ac.uk

Abstract

An emitter in the vicinity of a metal nanostructure is quenched by its decay through non-radiative channels, leading to the belief in a zone of inactivity for emitters placed within <10nm of a plasmonic nanostructure. Here we demonstrate that in tightly-coupled plasmonic resonators forming nanocavities "quenching is quenched" due to plasmon mixing. Unlike isolated nanoparticles, plasmonic nanocavities show mode hybridization which massively enhances emitter excitation and decay via radiative channels , experimentally confirmed by laterally dependent emitter placement through DNA-origami. This creates ideal conditions for realizing single-molecule strong-coupling with plasmons, evident in dynamic Rabi-oscillations.

Keywords

Nanoplasmonics, Nanophotonics, Light-matter Strong-coupling, Fluorescence Enhancement, Quenching

1 Introduction

The lifetime of an excited atomic state is determined by the properties of the atom and its environment, first theoretically suggested by Purcell [1] and followed by experimental demonstration by Goy et al. [2] Subsequent experiments further verified this by placing atomic emitters within various optical-field-enhancing geometries. [3–5] Plasmonic structures have the ability to massively enhance electromagnetic fields, and therefore dramatically alter the excitation rate of an emitter. [6] However, it is well known that, placing an emitter close to an isolated plasmonic nanostructure (< 10 nm), quenches its fluorescence. [7–9] Analysis by Anger et al. [6] showed this is due to the coupling of the emitter to non-radiative higher-order plasmonic modes that dissipate its energy. This 'zone of inactivity' was previously believed to quench all quantum emitters.

However, recent advancements have shown that an emitter's emission rate can be enhanced with plasmonic nano-antennas, [10–17] which efficiently converts far-field radiation into a localized field and vice versa. As first theoretically explained by Jun et al., [18] a single emitter placed into near-contact with a plasmonic nano-antenna can efficiently couple with the antenna's plasmonic modes and overcome quenching. [19,20] This was experimentally demonstrated by Hoang et al. [17] who showed that a quantum dot in a 12 nm nano-gap exhibits ultra-fast spontaneous emission. What however remains unclear is if this enhanced emission is strong enough to allow for single emitter strong coupling with plasmons.

In this article, we demonstrate and explain why quenching is substantially suppressed in plasmonic nanocavities, to such a degree that facilitates light-matter strong-coupling of a single-molecule at room-temperature as we recently demonstrated experimentally. [21,22] This

is due to: (i) the dramatic increase in the emitter excitation (similar to plasmonic antennas), and (ii) the changed nature of higher-order modes that acquire a radiative component, and therefore increase the quantum yield of the system. Modes in plasmonic nanocavities are not a simple superposition of modes from isolated structures, but instead are hybrid-plasmonic states.[23–27] Hence, higher-order modes that are dark for an isolated spherical nanoparticle, radiate efficiently for tightly-coupled plasmonic structures,[28] significantly reducing the non-radiative decay and quenching. By comparing an isolated nanoparticle (NP) with a nanoparticle-on-mirror (NPoM) nanocavity (equivalent alternatives being nanoparticle dimers with <3 nm gap), we quantify their different radiative and non-radiative channels, explaining the mechanism that leads to suppression of quenching in plasmonic nanocavities. We then experimentally demonstrate the suppression of quenching in plasmonic nanocavities, using DNA-origami to control the position of a single emitter in the nanogap. Finally, we complement our analysis by investigating the strong-coupling dynamics on the basis of a semi-classical Maxwell-Bloch description. We perform 3D Finite-Difference Time-Domain (FDTD) calculations to reveal the (spatio-temporal) emission dynamics in each system.

2 Suppressed fluorescence quenching

The fluorescence rate γ_{em} of an emitter generally depends on its excitation rate (γ_{exc}), and its radiative decay rate (i.e. quantum yield, $\eta = \gamma_{\mathrm{rad}}/\gamma_{\mathrm{tot}}$) as:[6]

$$\gamma_{\mathrm{em}} = \gamma_{\mathrm{exc}}\,\eta = \gamma_{\mathrm{exc}}\left(\frac{\gamma_{\mathrm{rad}}}{\gamma_{\mathrm{tot}}}\right) \tag{1}$$

where γ_{rad} and γ_{tot} are the emitter's radiative and total (Purcell factor) decay rates. The normalized excitation rate is governed by the field enhancement at the position of the emitter, and assuming that the environment does not affect the emitter's polarizability we have:

$$\tilde{\gamma}_{\mathrm{exc}} = \frac{\gamma_{\mathrm{exc}}}{\gamma^{0}_{\mathrm{exc}}} = \left|\frac{\hat{\boldsymbol{\mu}}\cdot\mathbf{E}(\mathbf{r}{=}0)}{\hat{\boldsymbol{\mu}}\cdot\mathbf{E}_0(\mathbf{r}{=}0)}\right|^2, \tag{2}$$

where $\hat{\boldsymbol{\mu}}$ is the emitter's polarizability unit vector, $\mathbf{E}(\mathbf{r}{=}0)$ is the total (incident and scattered) electric field and $\mathbf{E}_0(\mathbf{r}{=}0)$ the incident field at $\mathbf{r}{=}0$ where the emitter is placed. For simplicity, we assume that the emitter has no intrinsic loss, and hence the quantum yield of an emitter with radiative decay rate $\gamma_{\rm rad} = \gamma_{\rm tot} - \gamma_{\rm nr}$ is calculated by assuming that non-radiative decay is due to the Ohmic losses of the metal:[6] $\gamma_{\rm nr} \propto \int_V {\rm Re}\,\{\mathbf{j}(\mathbf{r}) \cdot \mathbf{E}^*_{\rm em}(\mathbf{r})\}\, d\mathbf{r}^3$, where $\mathbf{j}$ is the induced current density within the volume V and $\mathbf{E}_{\rm em}$ is the field emitted by the emitter.

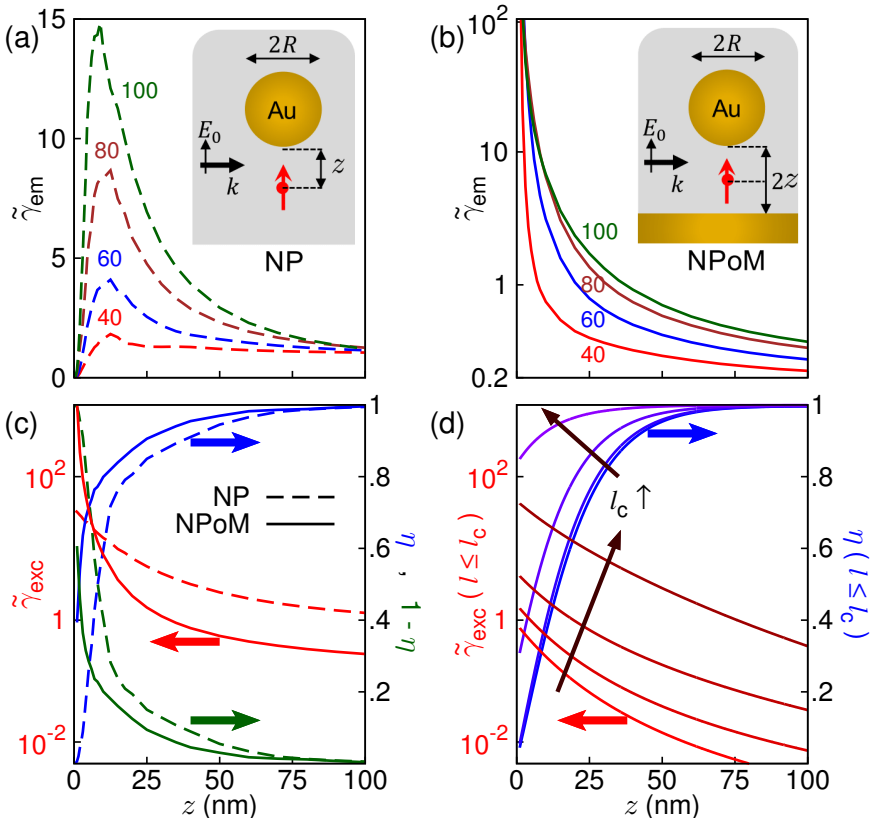

Figure 1: Fluorescence rate $\tilde{\gamma}_{\rm em}$ of an emitter with transition wavelength $\lambda_0 = 650$ nm placed at distance z from (a) an isolated NP and (b) inside the NPoM nanocavity, for sphere diameters $2R = 40$, 60, 80 and 100 nm and with background permittivity $\epsilon_D = 1.96$. (c) Excitation rate $\tilde{\gamma}_{\rm exc}$ (red), quantum yield η (blue) and $1-\eta$ (green) for an isolated NP (dashed lines) and a nanocavity (solid lines) of nanoparticle diameter 80 nm. (d) Coupling contributions to the excitation rate (red) and quantum yield (blue) when truncating the hybridization terms at $l_{\rm c} = 2$, 3, 5 and 10.

In the case of an isolated spherical nanoparticle (or a plasmonic nano-antenna), an emitter couples dominantly to the nanoparticle dipolar (first-order) mode. However as the emitter

approaches the nanoparticle, it couples increasingly to higher-order modes, which are dark. This leads to its energy dissipation via Ohmic losses (quenching). Fig. 1(a) shows the normalized fluorescence rate $\tilde{\gamma}_{\mathrm{em}} = \eta\,\tilde{\gamma}_{\mathrm{exc}}$ for an isolated NP, calculated for a classical dipole approaching the structure, using FDTD simulations. Quenching appears when the emitter is placed at $z < 10$ nm, in line with previously reported results.[6] By contrast, similar calculations for the NPoM nanocavity with the emitter always in the center of the nanocavity [Fig. 1(b)] reveal that the emission rate increases by several orders of magnitude (note the log-scale). As z decreases, the gap between nanoparticle and mirror reduces, and both plasmonic surfaces approach the emitter, but $\tilde{\gamma}_{\mathrm{em}}$ dramatically increases. Since the emission rate is a product of the excitation and radiative rates, we plot them separately [Fig. 1(c) and Fig.S1] for both an isolated NP and the nanocavity. As the emitter is progressively confined within the nanocavity, its excitation rate exponentially increases, due to the very high confinement of the plasmon modes within the gap. Additionally, the quantum yield (η) of the nanocavity out-performs the isolated NP by more than an order of magnitude as the gap decreases. While non-local effects can affect the quantitative rates of emission, excitation, and quantum yield of both structures at sub-nm spacings, no qualitative change is expected on their behaviour[29–31] (see S1.3 for more discussion).

To illuminate the origin of these different behaviours, we adapt the analytical description of coupled plasmon modes.[23,24] Isolated spherical nanoparticles are well dominated by Mie theory, but the problem of two coupled plasmonic nanoparticles is analytically more complex to determine. It has been solved in the quasi-static limit using several techniques, such as transformation optics[32–34] and multipole expansion.[25–27,35] However, it is more appropriate to formulate the problem as the coupling of the bare plasmonic modes from the two structures. Adapting this description for the NPoM (by approximating the mirror as a large sphere of radius r_m=1μm), the field enhancement in the middle of the nanocavity gap is given by:[23]

$$\frac{E(r{=}0)}{E_0} \simeq \alpha^{\mathrm{NP}} \left(\frac{R}{R+z}\right)^3 + \alpha^m \left[1 + \sum_{l=2}^{\infty} \frac{\sqrt{\omega_1 \omega_l}}{\omega_l - \omega - i\gamma/2} \left(\frac{l+1}{2}\right)^2 \frac{R^{(2l+1)}}{(R+z)^{(l+2)}\, r_m^{l-1}}\right],$$

where R is the radius of the nanoparticle, $2z$ is the gap size assuming the emitter is in the middle of the gap, and $\omega_l = \omega_p\sqrt{l/(2l+1)}$ is the resonant frequency of mode l, with ω_p and γ the metal plasmon frequency and damping. The nanoparticle quasi-static polarizability $\alpha^{\mathrm{NP}} = 2\frac{(\varepsilon_{\mathrm{Au}}-1)}{(\varepsilon_{\mathrm{Au}}+1)}$, while the mirror polarizability α^m is given by Mie scattering (beyond the quasi-static limit) in.[36] The first term provides the field enhancement contribution of the nanoparticle dipole mode, the first term in square brackets is the mirror dipole mode, and the second term in square brackets is the coupling of the mirror to the higher-order modes of the nanoparticle ($l \geq 2$). In Figure 1(d) we plot this latter contribution of the coupling terms in equation (3) to the excitation rate (red lines) while truncating at increasingly higher-order modes. As the nanocavity gets smaller ($z \downarrow$), higher-order mode hybridization is needed to account for the exponential increase of the NPoM excitation rate (seen in Fig. 1(c)). Similarly, the quantum yield increases with increasingly higher-order hybridization between the two structures. Both these demonstrate that the mode hybridization of the coupled plasmonic structures forming the nanocavity alter the fluorescence rate of an emitter in a way that fully suppresses quenching.

The spectral dependence of the radiative, total, and excitation rates for both the isolated NP and the nanocavity, varying the nanoparticle diameter from 20 nm to 100 nm, show strongly contrasting behaviour [Fig. 2]. Again the emitter is 0.5 nm from the Au surfaces, or at the centre of the 1 nm gap. Isolated quasi-static nanoparticles (with $2R < 100$ nm) possess diameter-independent modes [Fig. 2(a,c,e)]. However the resonant wavelengths of the nanocavity modes are highly dependent on the system geometry[28,37] [Fig. 2(b,d,f)]. The NPoM radiative decay rate $\tilde{\gamma}_{\mathrm{rad}} = \gamma_{\mathrm{rad}}/\gamma_0$, normalized to the free space decay rate γ_0, is three orders of magnitude larger than for the isolated NP, with the NPoM dipole ($l = 1$) mode significantly red-shifting for larger nanoparticles. Additionally the quadrupole NPoM mode ($l = 2$) strongly radiates and for larger nanoparticles has comparable radiative rates to the dipole ($l = 1$) mode, in great contrast with the isolated NP. These large $\tilde{\gamma}_{\mathrm{rad}}$ suppress quenching, and allow strong-coupling dynamics to be radiated into the far-field.

The Purcell factor (normalized total decay rate $\tilde{\gamma}_{\mathrm{tot}} = \gamma_{\mathrm{tot}}/\gamma_0$) for both plasmonic structures shows a diameter-independent broad peak at $\lambda_{\mathrm{pm}} \simeq 510$ nm [Fig. 2(c,d)], which corresponds to the superposition of multiple high-order plasmonic modes, recently referred to as a 'pseudo-mode'.[32,38] However, the negligible $\tilde{\gamma}_{\mathrm{rad}}$ at λ_{pm} shows the large $\tilde{\gamma}_{\mathrm{tot}}$ comes from emission coupled to the pseudo-mode decaying via non-radiative channels ($\tilde{\gamma}_{\mathrm{tot}} = \tilde{\gamma}_{\mathrm{rad}} + \tilde{\gamma}_{\mathrm{nr}}$). In contrast to recent proposals,[32] this suggests the nanocavity pseudo-mode quenches emission almost entirely via non-radiative channels, as it does for isolated nanoparticles, suppressing any way to observe possible strong-coupling dynamics. At the NPoM dipole and quadrupole resonant wavelengths, $\tilde{\gamma}_{\mathrm{rad}} \sim \tilde{\gamma}_{\mathrm{tot}}/2$, and therefore information of the coherent energy exchange between the emitter and the plasmon modes are carried to the far-field and thus allows tracking of the hybrid states.

Additionally, the excitation rate $\tilde{\gamma}_{\mathrm{exc}}$ of an emitter next to an isolated NP is two orders of magnitude smaller than for a 1 nm nanocavity [Fig. 2(e,f)]. Hence for an isolated NP where $\tilde{\gamma}_{\mathrm{rad}} \ll \tilde{\gamma}_{\mathrm{tot}}$, an emitter is weakly excited and heavily quenched by higher-order modes. On the other hand, the NPoM nanocavity strongly excites the emitter with the dipole/quadrupole modes, with $\tilde{\gamma}_{\mathrm{exc}}$ increasing for larger nanoparticles, but also significant energy is both radiated ($\tilde{\gamma}_{\mathrm{rad}} \sim \tilde{\gamma}_{\mathrm{tot}}/2$) and exchanged between the emitter and plasmons. Due to the mode hybridization and radiative behaviour of higher-order modes for the NPoM, its γ_{em} is dramatically increased and hence allows the room-temperature strong-coupling of a single emitter in plasmonic nanocavities to be experimentally measured.[21]

3 DNA-origami controlled fluorescence measurements

These findings are continued with experimental measurements, where we place a single Cy5 molecule within NPoM nanocavities formed by 80 nm diameter nanoparticles. DNA-origami[39] is used to create a 5 nm-thick spacer and to control the emitter position at nm lateral and vertical accuracies relative to the gold-nanoparticle [Fig. 3 inset]. A 2-layer DNA-

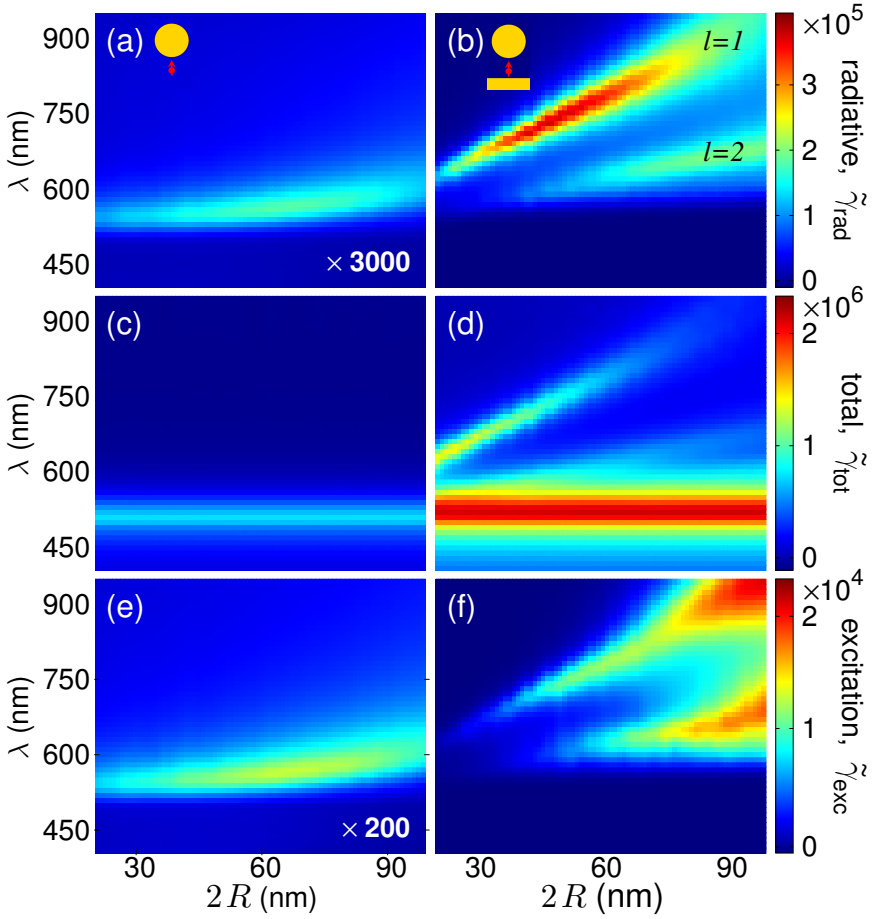

Figure 2: Spectra for a vertically-oriented emitter placed (a,c,e) 0.5 nm below an isolated NP, and (b,d,f) inside a 1 nm-wide NPoM nanocavity. (a,b) Normalized radiative decay rate $\tilde{\gamma}_{\mathrm{r}}$, (c,d) Normalized total decay rate $\tilde{\gamma}_{\mathrm{tot}}$ (Purcell factor), and (e,f) Normalized excitation rate $\tilde{\gamma}_{\mathrm{exc}}$.

origami plate (55×60 nm) is attached onto a gold substrate via thiol-modified staple strands. This is followed by hybridising ssDNA-functionalized gold nanoparticles with complementary overhang staple strands onto the top of the origami.[39] The position of the dye molecules with respect to the NP is varied by folding the origami with specific Cy5-modified staples at predefined positions from the centre of the NP attachment groups. We illuminate the nanocavity with a high numerical aperture (NA 0.8) objective, filling the back focal plane of the aperture with 633 nm laser light. The emission rates are extracted from luminescence at 690 nm from $>$ 300 individual NPoM cavities. These intensities are normalized to a control dye molecule on a glass substrate, see S2.1 for more detail. Note that the sub-ps emission

timescales here preclude any direct measurement of emission rates, for any position of the dye molecule, since current state-of-the-art equipment cannot resolve such fast decays.

The experimental emission rates at different lateral positions [Fig. 3, black points] quantitatively match the numerically-calculated emission rates for dipoles oriented along the z-axis and at 45°, as indicated. These results showing $\tilde{\gamma}_{\mathrm{em}}(|x|)$ combine both positive and negative x, which are identical [Fig. **??**], placing the x=0 particle centre within an experimental error of ±2 nm. Different DNA-origami foldings result in slightly different dipole orientations, and partial melting of the double-stranded DNA together with slight imprecision in nanoparticle placement yield the uncertainty in emitter position. These small variations lead to different emission intensities in different NPoMs, shown as vertical error bars in the experimental data [Fig. 3]. It is however evident that an emitter in a plasmonic nanocavity does not quench, even if it is placed in the vicinity (< 10 nm) of metal nanostructures, but instead its emission rate enhances.

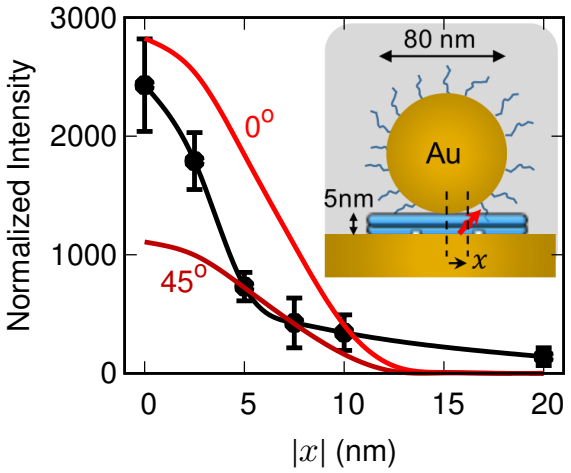

Figure 3: Experimental (black) and numerical (red) emission intensities of a single Cy5 molecule inside a DNA-origami structure with 5 nm nanocavity gap and 80 nm diameter. Molecule is laterally displaced by x from center of nanocavity and excited by a 633 nm laser. Inset: schematic diagram of the experimental setup where the Cy5 molecule is represented as a red arrow embeded within the DNA-origami, represented in blue.

4 Strong-coupling dynamics

The dramatically enhanced $\gamma_{\rm em}$ for NPoM is the reason that we can measure the strong-coupling dynamics at room temperature. While the classical calculations presented so far provide useful insight into the radiative and non-radiative decay channels of these differing plasmonic systems, they cannot reveal the spatio-temporal dynamics of an emitter coupling to the plasmons. We thus now use a dynamic two-level Maxwell-Bloch description[40] for the emitter, where the excited- (N_2) and ground- (N_1) state populations dynamics are described by:

$$\frac{\partial^2 \mathbf{P}}{\partial t^2} + 2\Gamma \frac{\partial \mathbf{P}}{\partial t} + (\Gamma^2 + \omega_0^2)\mathbf{P} = -\frac{2\omega_0}{\hbar}\mu^2 (N_2 - N_1)\mathbf{E}(t) \tag{3}$$

$$\frac{\partial N_2}{\partial t} = -\frac{\partial N_1}{\partial t} = -\gamma N_2 + \frac{1}{\hbar\omega_0}\left(\frac{\partial \mathbf{P}}{\partial t} + \Gamma \mathbf{P}\right) \cdot \mathbf{E}(t) \tag{4}$$

where $\mathbf{P}$ the induced polarization, $\omega_0 = 2\pi/\lambda_0$ the transition frequency, μ the transition dipole moment, and γ and Γ are the relaxation and dephasing rates of the emitter. Here, the parameters take realistic values from Ref. 21: $\mu = 3.79$D, $\gamma = 0.66$ μeV and $\Gamma = 28$ meV. In FDTD calculations, the simulation space is divided into a grid, and the plasmons (E-field) in each grid cell is obtained by solving the classical Maxwell equations. The polarization response $\mathbf{P}$ is driven by the two-level system and injects photons which can couple back to plasmons in a rigorous and self-consistent way. For more detail on Maxwell-Bloch description, see S3.1.

In Fig. 4(a), we plot the near-field $E_z(\mathbf{r}{=}0)$ time evolution after a broadband pulsed excitation without ($E_{\rm z}^{\rm cav}$, red) and with ($E_{\rm z}^{\rm em}$, blue) an emitter placed 0.5 nm from a nanoparticle of diameter 40 nm. The population of the excited state N_2 is also plotted on the same time-scale, which peaks at $\sim$ 20fs. A qualitatively similar behaviour is observed for the NPoM [Fig. 4(b)] but with 4 times stronger field enhancement and 200 times larger excited state population. To clearly demonstrate the induced E-field from the emitter $E_{\rm em}^{\rm ind} = E_{\rm z}^{\rm em} - E_{\rm z}^{\rm cav}$, we separate the field due to emitter-plasmon coupling $E_{\rm z}^{\rm em}$ from the field due to direct plasmon excitation $E_{\rm z}^{\rm cav}$. In Fig. 4(c,d), we plot $E_{\rm em}^{\rm ind}$ for emitters placed at various lateral

positions away from closest proximity to both the isolated NP and the NPoM. For emitters at $x < 5$ nm from the isolated NP, $E_{\rm em}^{\rm ind}$ reduces, despite the stronger field enhancement. This shows that energy from the emitter is quenched due to coupling with non-radiative higher-order modes that are confined to the vicinity of the isolated NP. For the NPoM, as the emitter approaches the nanocavity $E_{\rm em}^{\rm ind}$ is instead increasingly enhanced.

Similar behaviour is observed from the excited state population dynamics [Fig. 4(e,f)]. For $x < 2.5$ nm from the isolated NP, the population of the excited state is truncated by decay into the non-radiative channels, reducing it below that for an emitter at $x = 5$ nm, a behaviour not present for the NPoM cavity. The excited state life-times for both the isolated NP and the NPoM are shown in Fig. **??**, calculated both semi-classically and classically. This behaviour of extreme plasmonic nanocavities facilitates the strong-coupling of a single emitter at room temperature.

In fact, Rabi-oscillations can be observed long after the excitation pulse is turned off at $\sim$100 fs for the NPoM while almost entirely absent for the isolated NP as clearly shown on the envelope dynamics of $E_{\rm em}^{\rm ind}$ at $x = 0$ in Fig. 5. Therefore, for $t > 100$ fs, we observe the continuous energy exchange between the plasmon and an emitter. Due to the very dissipative nature of plasmons and the absence of continuous plasmon excitation, the Rabi oscillations are only visible on a log-scale as shown in Fig. 5(c) with period of $\sim$80 fs, which corresponds to the Rabi energy of $\sim$50 meV.

While Fig. 5 demonstrates the Rabi oscillations observed in the near-field from an emitter, to explore the far-field behaviour, we plot the scattering cross-sections for an emitter placed at lateral positions $x = 0$, 2.5, and 20 nm in Fig. 6(a,b) for both the isolated NP and NPoM. Scattering spectra of an isolated NP show no dependence on the emitter's position. This indicates that the far-field remains oblivion to the emitter as it mainly couples with the dark higher-order modes. However, for the NPoM nanocavity, the Rabi-splitting is observed when the emitter is well within the nanocavity which carries the characteristics of the energy exchange dynamics shown in Fig. 5(c). The maximum splitting at $x = 0$ corresponds to the

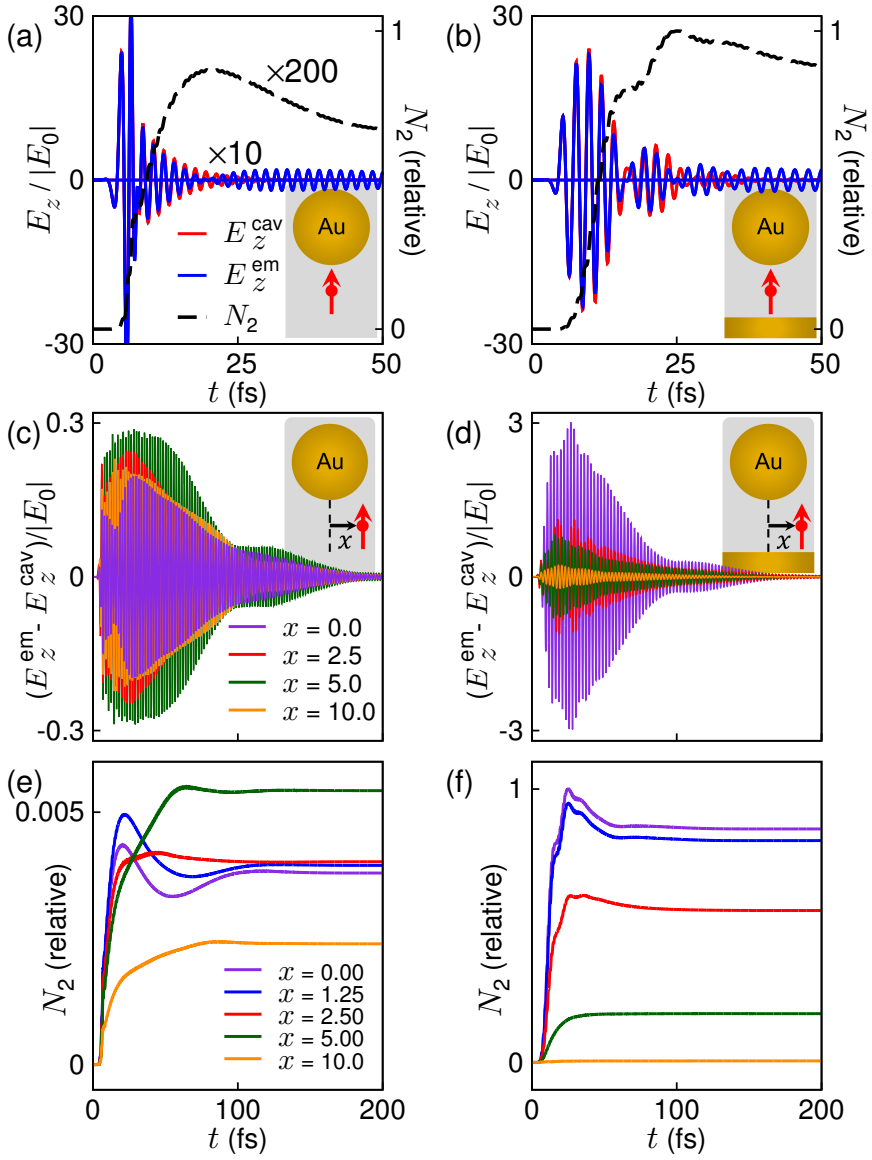

Figure 4: The field E_z and excited state population N_2 dynamics for (a,c,e) isolated NP and (b,d,f) 1 nm-wide NPoM of diameter 40 nm for a two-level emitter placed 0.5 nm below the nanoparticle. (a,b) E_z (red, blue) and N_2 (black) dynamics for the structures without (red) and with (blue) the presence of the emitter at $x = 0$. (c,d) The corresponding induced E-fields from the emitter $E_{\rm em}^{\rm ind} = E_z^{\rm em} - E_z^{\rm cav}$ and (e,f) the excited state population N_2 of the emitter, laterally displaced at $x = 0$, 1.25, 2.5, 5 and 10 nm. The emitters' transition wavelengths are $\lambda_0 = 550$ and 700 nm, tuned to the dipole plasmonic mode of each system.

Rabi energy of 66 meV, in comparison with ∼50 meV predicted by Fig. 5(c).

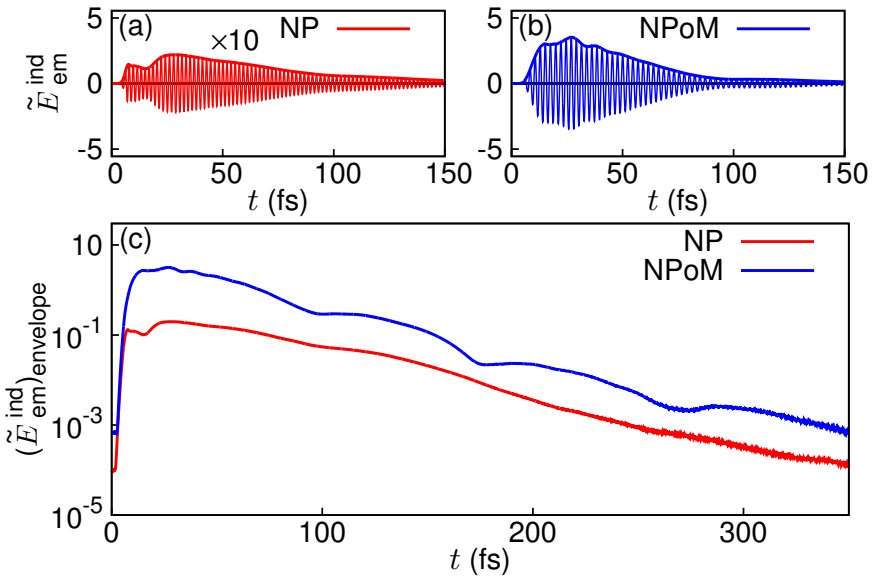

Figure 5: The nomalized induced field from an emitter $\tilde{E}^{\rm ind}_{\rm em} = (E^{\rm em}_z - E^{\rm cav}_z)/|E_0|$ for (a) an isolated NP (×10) and (b) the NPoM when the emitter is placed 0.5 nm below the nanoparticle. (c) The envelope dynamics of the induced field on log-scale, which demonstrates the Rabi oscillations.

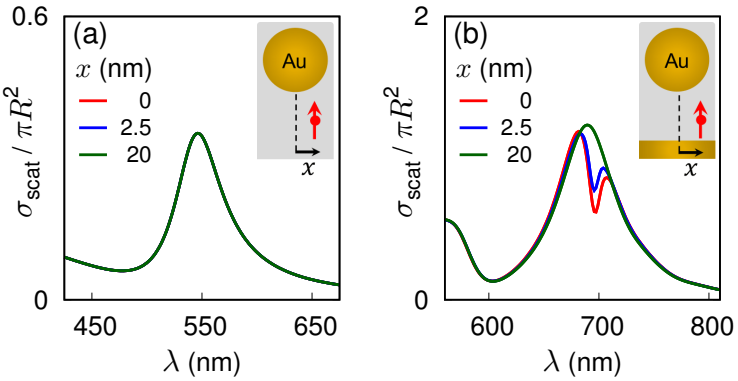

Figure 6: Scattering cross-sections for (a) an isolated NP and (b) NPoM, with the two-level quantum emitter placed placed 0.5 nm below the nanoparticle and laterally at x=0, 2.5, and 20 nm.

5 Conclusions

In conclusion, we have demonstrated analytically, numerically, and experimentally that an emitter placed within a plasmonic nanocavity does not quench, despite being in very close proximity to a metal nanoparticle. This is due to (i) the enhanced excitation always present in plasmonic antennas and (ii) the acquired radiative nature of higher-order modes for ex-

tremely small gaps. The combination of the two effects both suppresses the emitter's decay into non-radiative channels and facilitates the re-emission of its energy. Plasmonic nanocavities do not quench emitters, but instead provide the necessary conditions to achieve and observe single-molecule strong-coupling with plasmons at room temperature, and many other related light-matter interactions. Using semi-classical calculations, we show that the strong-coupling dynamics of single emitters in plasmonic nanocavities are fundamentally different from isolated nanoparticles and plasmonic nano-antennas with tens of nanometer gaps.

Acknowledgement

We acknowledge support from EPSRC grants EP/G060649/1 and EP/L027151/1 and European Research Council grant LINASS 320503. N.K. and A.D. contributed equally to this work.

Supporting Information Available

(1) Radiative, non-radiative and excitation enhancements of the nanocavities;(2) discussion on the nonlocal effects on the nanocavities; (3) additional detail on the experimental measurements; (4) normalization procedures of fluorescence intensities; (5) mode volume calculations; (6) theoretical decription of two-level Maxwell-Bloch model; (7) life-times of an emitter placed in the nanocavities; (8) far-field scattering cross-sections of the nanocavities.

This material is available free of charge via the Internet at `http://pubs.acs.org/`.

References

(1) Purcell, E. Spontaneous emission probabilities at radio frequencies. *Physical Review* **1946**, *69*, 681.

(2) Goy, P.; Haimond, J. M.; Gross, M.; Haroche, S. Observation of Cavity-Enhanced Single-Atom Spontaneous Emission. *Physical Review Letters* **1983**, *50*, 1903–1906.

(3) Drexhage, K. IV Interaction of Light with Monomolecular Dye Layers. *Progress in Optics* **1974**, *12*, 163–192.

(4) Kleppner, D. Inhibited Spontaneous Emission. *Physical Review Letters* **1981**, *47*, 233.

(5) Lodahl, P.; van Driel, A. F.; Nikolaeva, I. S.; Irman, A.; Overgaag, K.; Vanmaekelbergh, D.; Vos, W. L. Controlling the dynamics of spontaneous emission from quantum dots by photonic crystals. *Nature* **2004**, *430*, 654.

(6) Anger, P.; Bharadwaj, P.; Novotny, L. Enhancement and Quenching of Single-Molecule Fluorescence. *Physical Review Letters* **2006**, *96*, 113002.

(7) Dulkeith, E.; Morteani, A. C.; Niedereichholz, T.; Klar, T. A.; Feldmann, J.; Levi, S. A.; van Veggel, F. C. J. M.; Reinhoudt, D. N.; MÃűller, M.; Gittins, D. I. Fluorescence Quenching of Dye Molecules near Gold Nanoparticles: Radiative and Nonradiative Effects. *Physical Review Letters* **2002**, *89*, 203002.

(8) Kuhn, S.; Hakanson, U.; Rogobete, L.; Sandoghdar, V. Enhancement of Single-Molecule Fluorescence Using a Gold Nanoparticle as an Optical Nanoantenna. *Physical Review Letters* **2006**, *97*, 017402.

(9) Galloway, C. M.; Etchegoin, P. G.; Ru, E. C. L. Ultrafast Nonradiative Decay Rates on Metallic Surfaces by Comparing Surface-Enhanced Raman and Fluorescence Signals of Single Molecules. *Physical Review Letters* **2009**, *103*, 063003.

(10) Farahani, J. N.; Pohl, D. W.; Eisler, H.-J.; Hecht, B. Single Quantum Dot Coupled to a Scanning Optical Antenna: A Tunable Superemitter. *Physical Review Letters* **2005**, *95*, 017402.

(11) Muskens, O. L.; Giannini, V.; Sánchez-Gil, J. A.; Rivas, J. G. Strong Enhancement of the Radiative Decay Rate of Emitters by Single Plasmonic Nanoantennas. *Nano Letters* **2007**, *7*, 2871âĂŞ2875.

(12) Mohammadi, A.; Sandoghdar, V.; Agio, M. Gold nanorods and nanospheroids for enhancing spontaneous emission. *New Journal of Physics* **2008**, *10*, 105015.

(13) Kinkhabwala, A.; Yu, Z.; Fan, S.; Avlasevich, Y.; Mullen, K.; Moerner, W. E. Large single-molecule fluorescence enhancements produced by a bowtie nanoantenna. *Nature Photonics* **2009**, *3*, 654–657.

(14) Novotny, L.; van Hulst, N. Antennas for light. *Nature Photonics* **2011**, *5*, 83âĂŞ90.

(15) Biagioni, P.; Huang, J.-S.; Hecht, B. Nanoantennas for visible and infrared radiation. *Reports on Progress in Physics* **2012**, *75*, 024402.

(16) Pors, A.; Bozhevolnyi, S. I. Quantum Emitters near Layered Plasmonic Nanostructures: Decay Rate Contributions. *ACS Photonics* **2015**, *2*, 228âĂŞ236.

(17) Hoang, T. B.; Akselrod, G. M.; Mikkelsen, M. H. Ultrafast room-temperature single photon emission from quantum dots coupled to plasmonic nanocavities. *Nano Letters* **2016**, *16*, 270âĂŞ275.

(18) Jun, Y. C.; Kekatpure, R. D.; White, J. S.; Brongersma, M. L. Nonresonant enhancement of spontaneous emission in metal-dielectric-metal plasmon waveguide structures. *Physical Review B* **2008**, *78*, 153111.

(19) Faggiani, R.; Yang, J.; Lalanne, P. Quenching, Plasmonic, and Radiative Decays in Nanogap Emitting Devices. *ACS Photonics* **2015**, *2*, 1739.

(20) Yang, J.; Faggiani, R.; Lalanne, P. Light emission in nanogaps: overcoming quenching. *Nanoscale Horizons* **2016**, *1*, 11.

(21) Chikkaraddy, R.; de Nijs, B.; Benz, F.; Barrow, S. J.; Scherman, O. A.; Rosta, E.; Demetriadou, A.; Fox, P.; Hess, O.; Baumberg, J. J. Single-molecule strong coupling at room temperature in plasmonic nanocavities. *Nature* **2016**, *535*, 127.

(22) Santhosh, K.; Bitton, O.; Chuntonov, L.; Haran, G. Vacuum Rabi splitting in a plasmonic cavity at the single quantum emitter limit. *Nature communications* **2016**, *7*.

(23) Sun, G.; Khurgin, J. Comparative study of field enhancement between isolated and coupled metal nanoparticle: An analytical approach. *Applied Physics Letters* **2010**, *97*, 263110.

(24) Sun, G.; Khurgin, J. Theory of optical emission enhancement by coupled metal nanoparticles: An analytical approach. *Applied Physics Letters* **2011**, *98*, 113116.

(25) Norton, S. J.; Vo-Dinh, T. Optical response of linear chains of metal nanospheroids and nanospheroids. *Journal of Optical Society of America A* **2008**, *25*, 2767.

(26) Dhawan, A.; Norton, S. J.; Gerhold, M. D.; Vo-Dinh, T. Comparison of FDTD numerical computations and analytical multipole expansion method for plasmonics-active nanosphere dimers. *Optics Express* **2009**, *17*, 9688.

(27) Vo-Dinh, T.; Dhawan, A.; Norton, S. J.; Khoury, C. G.; Wang, H.-N.; Misra, V.; Gerhold, M. D. Plasmonic Nanoparticles and Nanowires: Design, Fabrication and Application in Sensing. *Journal of Physical Chemistry C* **2010**, *114*, 7480.

(28) Mertens, J.; Demetriadou, A.; Bowman, R. W.; Benz, F.; Kleemann, M. E.; Tserkezis, C.; Shi, Y.; Yang, H. Y.; Hess, O.; Aizpurua, J.; Baumberg, J. J. Tracking Optical Welding through Groove Modes in Plasmonic Nanocavities. *Nano Letters* **2016**, *16*, 5605.

(29) Tserkezis, C.; Mortensen, N. A.; Wubs, M. How nonlocal damping reduces plasmon-enhanced fluorescence in ultranarrow gaps. *Physical Review B* **2017**, *96*, 085413.

(30) Tserkezis, C.; Stefanou, N.; Wubs, M.; Mortensen, N. A. Molecular fluorescence enhancement in plasmonic environments: exploring the role of nonlocal effects. *Nanoscale* **2016**, *8*, 17532.

(31) Tserkezis, C.; Wubs, M.; Mortensen, N. A. Robustness of the Rabi Splitting under Nonlocal Corrections in Plexcitonics. *ACS Photonics* **2017**,

(32) Li, R.-Q.; Hernangomez-Perez, D.; Garcia-Vidal, F.; Fernandez-Dominguez, A. Transformation Optics Approach to Plasmon-Exciton Strong Coupling in Nanocavities. *Physical Review Letters* **2016**, *117*, 107401.

(33) Zhao, R.; Luo, Y.; Fernandez-Dominguez, A. I.; Pendry, J. B. Description of van der Waals Interactions Using Transformation Optics. *Physical Review Letters* **2013**, *111*, 033602.

(34) Luo, Y.; Zhao, R.; Pendry, J. B. van der Waals interactions at the nanoscale: The effects of nonlocality. *Proceedings of the National Academy of Sciences* **2014**, *111*, 18422.

(35) de Abajo, F. G. Multiple scattering of radiation in clusters of dielectrics. *Physical Review B* **1999**, *60*, 6086.

(36) Kuwata, H.; Tamaru, H.; Esumi, K.; Miyano, K. Resonant light scattering from metal nanoparticles: Practical analysis beyond Rayleigh approximation. *Applied Physics Letters* **2003**, *83*, 4625–4627.

(37) Tserkezis, C.; Esteban, R.; Sigle, D. O.; Mertens, J.; Herrmann, L. O.; Baumberg, J. J.; Aizpurua, J. Hybridization of plasmonic antenna and cavity modes: Extreme optics of nanoparticle-on-mirror nanogaps. *Physical Review A* **2015**, *92*, 053811.

(38) Delga, A.; Feist, J.; Bravo-Abad, J.; Garcia-Vidal, F. J. Quantum Emitters Near a Metal Nanoparticle: Strong Coupling and Quenching. *Physical Review Letters* **2014**, *112*, 253601.

(39) Thacker, V. V.; Herrmann, L. O.; Sigle, D. O.; Zhang, T.; Liedl, T.; Baumberg, J. J.; Keyser, U. F. DNA origami based assembly of gold nanoparticle dimers for surface-enhanced Raman scattering. *Nature Communications* **2014**, *5*, 3448.

(40) Boyd, R. W. *Non-linear Optics*; Elsevier: United States of America, 2008.